Adaptive Monopulse Approach With Joint Linear Constraints for Planar Array at Subarray Level

ZIYANG CHENG, Student Member, IEEE
ZISHU HE, Member, IEEE
XIANG DUAN
XUEJING ZHANG, Student Member, IEEE
University of Electronic Science and Technology of China, Chengdu, China

BIN LIAO, Senior Member, IEEE
Shenzhen University, Shenzhen, China

This paper investigates the problem of angle measuring of the target in the presence of jammings with planar arrays. The relationship between the quiescent monopulse ratios and azimuth/elevation is first studied. On this basis, the distortion of the surface of the conventional minimum variance distortionless response monopulse ratio is analyzed. In order to avoid such distortion and approximate the adaptive monopulse ratio surface to the quiescent one, an adaptive monopulse approach with joint linear constraints on both the azimuth and elevation is proposed. Simulation results demonstrate that the proposed approach is capable of attaining a high angle measuring accuracy in the presence of mainlobe jammer.

Manuscript received July 17, 2016; revised March 20, 2017, July 22, 2017, and November 8, 2017; released for publication November 22, 2017. Date of publication January 15, 2018; date of current version June 7, 2018.

DOI. No. 10.1109/TAES.2018.2793318

Refereeing of this contribution was handled by A. Charlish.

This work was supported by the Fundamental Research Funds of Central Universities under Grant ZYGX2016J027.

Authors' addresses: Z. Cheng, Z. He, X. Duan, and X. Zhang are with the School of Electronic Engineering, University of Electronic Science and Technology of China, Chengdu 611731, China, E-mail: (zshe@uestc.edu.cn; cameldx@163.com; xjzhang7@163.com); B. Liao is with the College of Information Engineering, Shenzhen University, Shenzhen 518060, China, E-mail: (binliao@szu.edu.cn). *(Corresponding author: Ziyang Cheng.)*

I. INTRODUCTION

Adaptive arrays are very effective in improving the signal-to-interference-plus-noise ratio (SINR) in the case of external jamming [1], [2]. However, it should be noted that the shape of the sum and difference beam may be distorted because of the adaption. More importantly, this distortion would lead to angle measuring performance degradation, especially when jammers are close to the main beam [3].

In order to reduce the distortion, three different monopulse correction formulas based on maximum likelihood estimation (MLE) for uniform linear array (ULA) have been presented by Davies *et al.* [4]. To find the global optimal solution, a fine grid search that leads to high computational complexity is usually required. Hence, an adaptive monopulse algorithm, which can be regarded as the first-order Taylor approximation of the MLE, has been proposed to reduce the computational complexity [5], [6]. In [7] and [8], correction values for the slope and bias of the adaptive monopulse ratio have been derived. However, since the corrected monopulse method is a first-order Taylor approximation of the monopulse ratio, the angle measuring precision of this method is high when the angle of the target is at the vicinity of the antenna look direction, whereas it would be declined when the target locates in the mainlobe but significantly deviates from the look direction. To this end, the corrected monopulse method has been extended to antennas with low sidelobe patterns and digital beamforming with subarrays [9]–[11]. Furthermore, it has been shown that these methods are applicable to space-time adaptive processing [12]–[16].

In [17], a radar digital beamforming architecture, consisting of a sidelobe jamming canceling adaptive array followed by a mainlobe jamming canceller, is developed for nulling the jammers while maintaining the monopulse angle estimation accuracy. On the other hand, Fante developed another adaptive monopulse algorithm based on linear constraints of multipoints for ULA in [18]. With this method, the distortion of monopulse ratio can be effectively reduced. However, this method is not suitable for planar arrays, owing to the fact that the monopulse ratio depends on both azimuth and elevation. More recently, a constrained monopulse algorithm was proposed in [19] in the linear array case. Its extension to planar arrays was designed to make the estimation of one angle independent on the value of the other by adding constraints [19, eq. (30)] in comparison with the linear array case. However, in the noise only case, the optimal quiescent monopulse ratios [5] do depend on azimuth and elevation jointly. As a result, optimal angle measuring performance are unlikely to be guaranteed for all locations within the mainlobe region with the algorithm proposed in [19].

Motivated by the limitations of existing methods for angle estimation with planar arrays in the presence of jammings, this paper presents a new approach with joint linear constraints. More precisely, constraints on both of the azimuth and elevation monopulse ratios are imposed such that the resulting adaptive monopulse ratio surfaces are

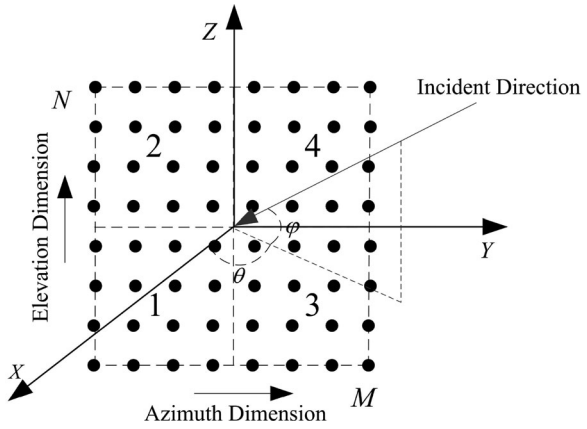

Fig. 1. Schematic diagram of planar phased array.

approximately equal to the quiescent monopulse ratio surfaces. To facilitate the development of the proposed method, the relationship between the quiescent monopulse ratios with the azimuth and elevation angles is first discussed. Moreover, the conventional minimum variance distortionless response (MVDR) monopulse approach is analyzed. In order to demonstrate the effectiveness of the proposed method and its superiority over conventional approaches, extensive simulation results under various situations are provided.

The remainder of this paper is organized as follows. The signal model and quiescent monopulse ratios are presented in Section II. In Section III, the distortion of surface of the conventional MVDR monopulse ratio is analyzed. The new approach with joint linear constraints is then developed in Section IV. Section V presents various simulation results and conclusions are finally drawn in Section VI.

Notations: Matrices and vectors are denoted by boldfaced capital and lower case letters, respectively. $(\cdot)^T$ and $(\cdot)^H$ are the transpose and complex conjugate transpose operators, respectively. $\Re\{\cdot\}$ and $\Im\{\cdot\}$ represent the real part and imaginary part of a complex number, respectively. $\otimes$ and $\odot$ stand for Kronecker product and Hadamard product, respectively. $\mathcal{C}^n$ denotes the sets of n-dimensional complex vectors.

II. SIGNAL MODEL AND QUIESCENT MONOPULSE RATIO

Consider a rectangular planar array with $M \times N$ elements in the Y–Z plane of a (x, y, z) coordinate reference system, and the normal direction of the planar array is X-axis as shown in Fig. 1. The array is partitioned into $L_1 \times L_2$ subarrays, in each of which the number of elements is $K_1 \times K_2$. Moreover, we have $K_1 \times L_1 = M$ and $K_2 \times L_2 = N$. It should be pointed out that this work focuses on a rectangular array with subarrays of equal size. Nevertheless, the proposed method can be extended to general planar arrays and the achievable angle measuring accuracy will depend on the array configuration.

The target angle is defined by the angular coordinates (θ, φ) corresponding to the azimuth and elevation. The direction cosines of the angle of incidence for azimuth u and elevation v can be written as

$$u = \sin\theta\cos\varphi \tag{1a}$$

$$v = \sin\varphi. \tag{1b}$$

The array output of the antenna elements, $\boldsymbol{x}$, is composed of the target echo plus interference $\boldsymbol{j}$ and receiver Gaussian white noise $\boldsymbol{n}$ as

$$\boldsymbol{x} = b\boldsymbol{a}(\theta, \varphi) + \boldsymbol{j} + \boldsymbol{n} \tag{2}$$

where the complex number b contains the target amplitude and phase, and $\boldsymbol{a}(\theta, \varphi)$ represents the MN-dimensional steering vector as

$$\boldsymbol{a}(\theta, \varphi) = [1\, e^{j\phi_{0\times 1}} \cdots e^{j\phi_{0\times N-1}} \cdots e^{j\phi_{M-1\times N-1}}]^T \tag{3}$$

where $\phi_{m\times n}$ is given by

$$\phi_{m\times n} = \frac{2\pi}{\lambda}(md_y u + nd_z v) \tag{4}$$

with d_y and d_z denoting the element spacings along the Y-axis and Z-axis, respectively, and λ being the carrier wavelength.

To proceed, let us denote all subarray outputs as an L_1L_2-dimensional vector $\boldsymbol{z}$, which can be equivalently transformed from the array output $\boldsymbol{x}$ with an $MN \times L_1L_2$ matrix $\boldsymbol{T}$ as

$$\boldsymbol{z} = \boldsymbol{T}^H\boldsymbol{x} \in \mathcal{C}^{L_1L_2} \tag{5}$$

where $\boldsymbol{T}$ can be written as

$$\boldsymbol{T} = \boldsymbol{T}_u \otimes \boldsymbol{T}_v \tag{6}$$

where the ith column of $\boldsymbol{T}_u$ (or $\boldsymbol{T}_v$) contains the complex weights for summing up the elements within the ith subarray in the azimuth (or elevation). More exactly, we have

$$\boldsymbol{T}_u = \begin{pmatrix} (g_1)_1 & 0 & \cdots & 0 \\ \vdots & \vdots & & \vdots \\ (g_1)_{K_1} & 0 & \cdots & \vdots \\ 0 & (g_2)_1 & & \vdots \\ \vdots & \vdots & \ddots & \vdots \\ \vdots & (g_2)_{K_1} & & 0 \\ \vdots & 0 & \cdots & (g_{L_1})_1 \\ \vdots & \vdots & & \vdots \\ 0 & 0 & \cdots & (g_{L_1})_{K_1} \end{pmatrix} \tag{7}$$

where $(g_i)_k = e^{j2\pi(k-1)d_y u_0/\lambda}$ with $i = 1, 2, \ldots, L_1$ and $k = 1, 2, \ldots, K_1$ denotes the complex weight of the kth element of the ith subarray in the azimuth. Here, $u_0 = \sin\theta_0\cos\varphi_0$ and (θ_0, φ_0) is the beam steering angle.

Similarly, the matrix $\boldsymbol{T}_v$ is given by

$$\boldsymbol{T}_v = \begin{pmatrix} (h_1)_1 & 0 & \cdots & 0 \\ \vdots & \vdots & & \vdots \\ (h_1)_{K_2} & 0 & \cdots & \vdots \\ 0 & (h_2)_1 & & \vdots \\ \vdots & \vdots & \ddots & \vdots \\ \vdots & (h_2)_{K_2} & & 0 \\ \vdots & 0 & \cdots & (h_{L_2})_1 \\ \vdots & \vdots & & \vdots \\ 0 & 0 & \cdots & (h_{L_2})_{K_2} \end{pmatrix} \tag{8}$$

where $(h_i)_k = e^{j2\pi(k-1)d_z v_0/\lambda}$ with $i = 1, 2, \ldots, L_2$ and $k = 1, 2, \ldots, K_2$ and $v_0 = \sin\varphi_0$ stands for the complex weight of the kth element of the ith subarray in the elevation.

In the case where only pure noise exists, a conventional monopulse system for angle estimation of the target typically consists of four quadrant identical antennas as shown in Fig. 1. Accordingly, the output of the sum beam r_{Σ}, output of the azimuth difference beam $r_{\Delta a}$, and output of the elevation difference beam $r_{\Delta e}$ can be written as

$$r_{\Sigma} = \boldsymbol{w}_{q\Sigma}^H \boldsymbol{z} \tag{9a}$$

$$r_{\Delta a} = \boldsymbol{w}_{q\Delta a}^H \boldsymbol{z} \tag{9b}$$

$$r_{\Delta e} = \boldsymbol{w}_{q\Delta e}^H \boldsymbol{z} \tag{9c}$$

where $\boldsymbol{w}_{q_\Sigma}$, $\boldsymbol{w}_{q_{\Delta a}}$, and $\boldsymbol{w}_{q_{\Delta e}}$ denote the quiescent sum beam weight, quiescent azimuth difference beam weight, and quiescent elevation difference beam weight, respectively. In particular, they can be expressed as

$$\boldsymbol{w}_{q\Sigma} = \boldsymbol{T}^H \boldsymbol{a}(\theta_0, \varphi_0) \tag{10}$$

$$\boldsymbol{w}_{q\Delta a} = \left([\overbrace{1, \ldots, 1}^{L_1/2}, \overbrace{-1, \ldots, -1}^{L_1/2}] \otimes [\overbrace{1, \ldots, 1}^{L_2}] \right) \odot \boldsymbol{w}_{q\Sigma} \tag{11}$$

$$\boldsymbol{w}_{q\Delta e} = \left([\overbrace{1, \ldots, 1}^{L_1}] \otimes [\overbrace{1, \ldots, 1}^{L_2/2}, \overbrace{-1, \ldots, -1}^{L_2/2}] \right) \odot \boldsymbol{w}_{q\Sigma}. \tag{12}$$

In a noiseless scenario, if the angle of the target (θ, φ) is in the neighborhood of the look direction (θ_0, φ_0), i.e., $(\theta, \varphi) = (\theta_0 + \Delta\theta, \varphi_0 + \Delta\varphi)$ with small angle deflections $\Delta\theta$ and $\Delta\varphi$, the approximated monopulse ratios are linearly related to the angle deflections [5], [17]. More specifically, we have

$$f_{qe} = \Im\left\{ \frac{\boldsymbol{w}_{q\Delta e}^H \tilde{\boldsymbol{a}}(\theta, \varphi)}{\boldsymbol{w}_{q\Sigma}^H \tilde{\boldsymbol{a}}(\theta, \varphi)} \right\} \approx \frac{\pi M d_y}{\lambda} \cos\varphi_0 \Delta\varphi \tag{13a}$$

$$f_{qa} = \Im\left\{ \frac{\boldsymbol{w}_{q\Delta a}^H \tilde{\boldsymbol{a}}(\theta, \varphi)}{\boldsymbol{w}_{q\Sigma}^H \tilde{\boldsymbol{a}}(\theta, \varphi)} \right\} \approx \frac{\pi N d_z}{\lambda} (\cos\theta_0 \cos\varphi_0 \Delta\theta - \sin\theta_0 \sin\varphi_0 \Delta\varphi) \tag{13b}$$

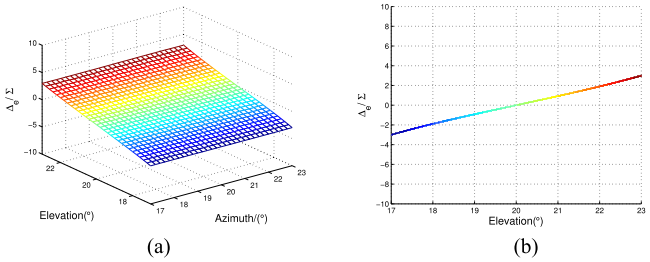

(a) (b)

Fig. 2. Surface of quiescent elevation monopulse ratio. (a) Oblique view. (b) Side view.

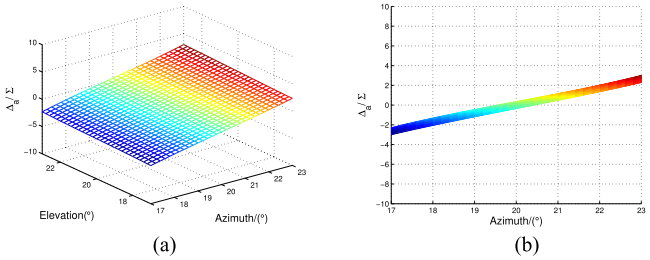

(a) (b)

Fig. 3. Surface of quiescent azimuth monopulse ratio. (a) Oblique view. (b) Side view.

where $\tilde{\boldsymbol{a}}(\theta, \varphi)$ is defined as

$$\tilde{\boldsymbol{a}}(\theta, \varphi) = \boldsymbol{T}^H \boldsymbol{a}(\theta, \varphi). \tag{14}$$

Notice that the quiescent monopulse ratios in (13) can be re-expressed in more compact forms as

$$f_{qe} = k_1 \Delta\varphi \tag{15a}$$

$$f_{qa} = k_2 \Delta\theta + k_3 \Delta\varphi \tag{15b}$$

where the coefficients k_1, k_2, and k_3 are given by

$$k_1 = \frac{\pi M d_y}{\lambda} \cos\varphi_0$$

$$k_2 = \frac{\pi N d_z}{\lambda} \cos\theta_0 \cos\varphi_0$$

$$k_3 = -\frac{\pi N d_z}{\lambda} \sin\theta_0 \sin\varphi_0. \tag{16}$$

Obviously, it is seen that the quiescent elevation monopulse ratio f_{qe} is only a linear function of $\Delta\varphi$, whereas the quiescent azimuth monopulse ratio f_{qa} depends on $\Delta\theta$ as well as $\Delta\varphi$.

In order to have a better understanding of the above results, a planar array of 16×16 elements spaced by half-wavelength is considered for illustration. The 3-dB beamwidth of the array is $(6.4°, 6.4°)$ and the look direction is $(20°, 20°)$. Figs. 2 and 3 depict the resulting surfaces of quiescent monopulse ratios. As expected, it can be observed from Fig. 2(b) that the elevation monopulse ratio is only linearly related to the elevation. However, Fig. 3(b) illustrates that the azimuth monopulse ratio is linear with azimuth and elevation.

III. ANALYSIS OF THE MVDR MONOPULSE APPROACH

Now, we analyze the distortion of the surface of the conventional MVDR monopulse ratio. It is known that the sum beam weight based on MVDR (after omitting the immaterial constant $\mu = 1/\boldsymbol{w}_{q_\Sigma}^H \boldsymbol{R}_{\text{sub}}^{-1} \boldsymbol{w}_{q_\Sigma}$) is given by [20], [21]

$$\boldsymbol{w}_{_\Sigma} = \boldsymbol{R}_{\text{sub}}^{-1} \boldsymbol{w}_{q_\Sigma} \tag{17}$$

where $\boldsymbol{R}_{\text{sub}}$ is the array covariance matrix. Owing to the finite observation time in practice, the exact knowledge of $\boldsymbol{R}_{\text{sub}}$ is unavailable. Instead, the following sample covariance matrix $\hat{\boldsymbol{R}}_{\text{sub}}$ is usually employed

$$\hat{\boldsymbol{R}}_{\text{sub}} = \frac{1}{K} \sum_{k=1}^{K} \boldsymbol{z}(k) \boldsymbol{z}^H(k) \tag{18}$$

where K denotes the training sample size.

Analogous to conventional quiescent monopulse processing, the azimuth difference beam weight and elevation difference beam weight can be written as

$$\boldsymbol{w}_{_{\Delta a}} = \hat{\boldsymbol{R}}_{\text{sub}}^{-1} \boldsymbol{w}_{q_{\Delta a}} \tag{19a}$$

$$\boldsymbol{w}_{_{\Delta e}} = \hat{\boldsymbol{R}}_{\text{sub}}^{-1} \boldsymbol{w}_{q_{\Delta e}}. \tag{19b}$$

As a consequence, the ratio of the sum to difference beam can be expressed as

$$f_e = \Im \left\{ \frac{\boldsymbol{w}_{\Delta e}^H \tilde{\boldsymbol{a}}(\theta, \varphi)}{\boldsymbol{w}_\Sigma^H \tilde{\boldsymbol{a}}(\theta, \varphi)} \right\} = \Im \left\{ \frac{\boldsymbol{w}_{q\Delta e}^H \hat{\boldsymbol{R}}_{\text{sub}}^{-1} \tilde{\boldsymbol{a}}(\theta, \varphi)}{\boldsymbol{w}_{q\Sigma}^H \hat{\boldsymbol{R}}_{\text{sub}}^{-1} \tilde{\boldsymbol{a}}(\theta, \varphi)} \right\} \tag{20a}$$

$$f_a = \Im \left\{ \frac{\boldsymbol{w}_{\Delta a}^H \tilde{\boldsymbol{a}}(\theta, \varphi)}{\boldsymbol{w}_\Sigma^H \tilde{\boldsymbol{a}}(\theta, \varphi)} \right\} = \Im \left\{ \frac{\boldsymbol{w}_{q\Delta a}^H \hat{\boldsymbol{R}}_{\text{sub}}^{-1} \tilde{\boldsymbol{a}}(\theta, \varphi)}{\boldsymbol{w}_{q\Sigma}^H \hat{\boldsymbol{R}}_{\text{sub}}^{-1} \tilde{\boldsymbol{a}}(\theta, \varphi)} \right\}. \tag{20b}$$

Careful examination of the equations in (20) and (13) shows that the conventional MVDR monopulse ratios are equal to the quiescent monopulse ratios when $\hat{\boldsymbol{R}}_{\text{sub}}$ is the identity matrix, i.e., when the samples for covariance matrix estimation contain noise only and the sample size is enough [22]. However, such equivalence does not hold true when the training samples contain jammings and noise . This implies that the surfaces of the conventional MVDR monopulse ratios will be distorted. Furthermore, the closer the jamming is to the look direction, the more distortion there is. Note that the equivalence may also be distorted due to small sample size even in absence jammers. In this case, the regularization (diagonal loading) principle [23] can be employed to penalize the imperfection.

IV. PROPOSED ADAPTIVE MONOPULSE APPROACH

In this section, a new approach with joint linear constraints to improve the angle estimation performance for planar arrays is presented. In this method, the sum beam weight obtained with MVDR will be exploited to determine the adaptive azimuth and elevation difference beam weights, which are required not only to minimize the power of the received jammings and noise, but also to guarantee the approximation between the adaptive and conventional quiescent monopulse ratios.

Let $\hat{f}_a(\theta, \varphi)$ and $\hat{f}_e(\theta, \varphi)$ denote the adaptive azimuth and elevation difference monopulse ratios, respectively. More specifically, they can be written as

$$\hat{f}_a(\theta, \varphi) = \frac{\Delta_a(\theta, \varphi)}{\Sigma(\theta, \varphi)} \tag{21a}$$

$$\hat{f}_e(\theta, \varphi) = \frac{\Delta_e(\theta, \varphi)}{\Sigma(\theta, \varphi)} \tag{21b}$$

where $\Sigma(\theta, \varphi)$ stands for the adaptive sum beam, $\Delta_a(\theta, \varphi)$ and $\Delta_e(\theta, \varphi)$ are the adaptive azimuth and elevation difference beams, respectively. In particular, we have

$$\Sigma(\theta, \varphi) = \boldsymbol{w}_\Sigma^H \tilde{\boldsymbol{a}}(\theta, \varphi) \tag{22a}$$

$$\Delta_a(\theta, \varphi) = \bar{\boldsymbol{w}}_{\Delta a}^H \tilde{\boldsymbol{a}}(\theta, \varphi) \tag{22b}$$

$$\Delta_e(\theta, \varphi) = \bar{\boldsymbol{w}}_{\Delta e}^H \tilde{\boldsymbol{a}}(\theta, \varphi) \tag{22c}$$

where $\boldsymbol{w}_\Sigma$ has been defined earlier in (17), $\bar{\boldsymbol{w}}_{\Delta a}$ and $\bar{\boldsymbol{w}}_{\Delta e}$ are the adaptive azimuth and elevation difference weights to be determined.

With the above notations and assuming that the look direction is (θ_0, φ_0) and the constraint interval is $(\Delta\theta', \Delta\varphi')$, then the monopulse ratios with respect to $(\theta_0 \pm \Delta\theta', \varphi_0 \pm \Delta\varphi')$ are given by

$$\hat{f}_a\left(\theta_0 \pm \Delta\theta', \varphi_0 \pm \Delta\varphi'\right) = \frac{\Delta_a\left(\theta_0 \pm \Delta\theta', \varphi_0 \pm \Delta\varphi'\right)}{\Sigma\left(\theta_0 \pm \Delta\theta', \varphi_0 \pm \Delta\varphi'\right)} \tag{23a}$$

$$\hat{f}_e\left(\theta_0 \pm \Delta\theta', \varphi_0 \pm \Delta\varphi'\right) = \frac{\Delta_e\left(\theta_0 \pm \Delta\theta', \varphi_0 \pm \Delta\varphi'\right)}{\Sigma\left(\theta_0 \pm \Delta\theta', \varphi_0 \pm \Delta\varphi'\right)}. \tag{23b}$$

In order to guarantee the approximation between the adaptive and conventional quiescent monopulse ratios, according to (15), the following conditions should be satisfied:

$$\frac{\Delta_a\left(\theta_0 \pm \Delta\theta', \varphi_0 \pm \Delta\varphi'\right)}{\Sigma\left(\theta_0 \pm \Delta\theta', \varphi_0 \pm \Delta\varphi'\right)} = \pm k_2 \Delta\theta' \pm k_3 \Delta\varphi' \tag{24a}$$

$$\frac{\Delta_e\left(\theta_0 \pm \Delta\theta', \varphi_0 \pm \Delta\varphi'\right)}{\Sigma\left(\theta_0 \pm \Delta\theta', \varphi_0 \pm \Delta\varphi'\right)} = \pm k_1 \Delta\varphi'. \tag{24b}$$

Hence, substituting (22) into (24), it is known that the adaptive azimuth and elevation difference weights $\hat{\boldsymbol{w}}_{\Delta a}$ and $\hat{\boldsymbol{w}}_{\Delta e}$ should be constrained as

$$\bar{\boldsymbol{w}}_{\Delta a}^H \tilde{\boldsymbol{a}}\left(\theta_0 \pm \Delta\theta', \varphi_0 + \Delta\varphi'\right) = \left(\pm k_2 \Delta\theta' \pm k_3 \Delta\varphi'\right) \boldsymbol{w}_\Sigma^H \tilde{\boldsymbol{a}}\left(\theta_0 \pm \Delta\theta', \varphi_0 + \Delta\varphi'\right) \tag{25a}$$

$$\bar{\boldsymbol{w}}_{\Delta e}^H \tilde{\boldsymbol{a}}\left(\theta_0 \pm \Delta\theta', \varphi_0 + \Delta\varphi'\right) = \left(\pm k_1 \Delta\varphi'\right) \boldsymbol{w}_\Sigma^H \tilde{\boldsymbol{a}}\left(\theta_0 \pm \Delta\theta', \varphi_0 + \Delta\varphi'\right). \tag{25b}$$

Notice that the above equalities can be written in compact forms as

$$\hat{\boldsymbol{w}}_{\Delta a}^H \boldsymbol{H} = \boldsymbol{\rho}_a \tag{26a}$$

$$\hat{\boldsymbol{w}}_{\Delta e}^H \boldsymbol{H} = \boldsymbol{\rho}_e \tag{26b}$$

where $\boldsymbol{H}$, $\boldsymbol{\rho}_a$, and $\boldsymbol{\rho}_e$ are defined as

$$\boldsymbol{H} = [\boldsymbol{H}_{\theta_0+\Delta\theta'} \quad \boldsymbol{H}_{\theta_0} \quad \boldsymbol{H}_{\theta_0-\Delta\theta'}] \tag{27}$$

$$\boldsymbol{\rho}_a = [\boldsymbol{\rho}_{a(\theta_0+\Delta\theta')} \quad \boldsymbol{\rho}_{a(\theta_0)} \quad \boldsymbol{\rho}_{a(\theta_0-\Delta\theta')}] \tag{28}$$

$$\boldsymbol{\rho}_e = [\boldsymbol{\rho}_{e(\theta_0+\Delta\theta')} \quad \boldsymbol{\rho}_{e(\theta_0)} \quad \boldsymbol{\rho}_{e(\theta_0-\Delta\theta')}] \tag{29}$$

with the subscripts $(\cdot)_{\theta_0+\Delta\theta'}$, $(\cdot)_{\theta_0}$, and $(\cdot)_{\theta_0-\Delta\theta'}$ denoting three azimuth constraint locations. The submatrices and subvectors in (27)–(29) are given by

$$\boldsymbol{H}_{\theta_0+\Delta\theta'} = \begin{bmatrix} \tilde{\boldsymbol{a}}^T\left(\theta_0+\Delta\theta', \varphi_0+\Delta\varphi'\right) \\ \tilde{\boldsymbol{a}}^T\left(\theta_0+\Delta\theta', \varphi_0\right) \\ \tilde{\boldsymbol{a}}^T\left(\theta_0+\Delta\theta', \varphi_0-\Delta\varphi'\right) \end{bmatrix}^T \tag{30}$$

$$\boldsymbol{H}_{\theta_0} = \begin{bmatrix} \tilde{\boldsymbol{a}}^T\left(\theta_0, \varphi_0+\Delta\varphi'\right) \\ \tilde{\boldsymbol{a}}^T\left(\theta_0, \varphi_0\right) \\ \tilde{\boldsymbol{a}}^T\left(\theta_0, \varphi_0-\Delta\varphi'\right) \end{bmatrix}^T \tag{31}$$

$$\boldsymbol{H}_{\theta_0-\Delta\theta'} = \begin{bmatrix} \tilde{\boldsymbol{a}}^T\left(\theta_0-\Delta\theta', \varphi_0+\Delta\varphi'\right) \\ \tilde{\boldsymbol{a}}^T\left(\theta_0-\Delta\theta', \varphi_0\right) \\ \tilde{\boldsymbol{a}}^T\left(\theta_0-\Delta\theta', \varphi_0-\Delta\varphi'\right) \end{bmatrix}^T \tag{32}$$

$$\boldsymbol{\rho}_{a(\theta_0+\Delta\theta')} = \begin{bmatrix} \left(k_2\Delta\theta'+k_3\Delta\varphi'\right)\boldsymbol{w}_\Sigma^H\tilde{\boldsymbol{a}}\left(\theta_0+\Delta\theta', \varphi_0+\Delta\varphi'\right) \\ \left(k_2\Delta\theta'\right)\boldsymbol{w}_\Sigma^H\tilde{\boldsymbol{a}}\left(\theta_0+\Delta\theta', \varphi_0\right) \\ \left(k_2\Delta\theta'-k_3\Delta\varphi'\right)\boldsymbol{w}_\Sigma^H\tilde{\boldsymbol{a}}\left(\theta_0+\Delta\theta', \varphi_0-\Delta\varphi'\right) \end{bmatrix}^T \tag{33}$$

$$\boldsymbol{\rho}_{a(\theta_0)} = \begin{bmatrix} \left(k_3\Delta\varphi'\right)\boldsymbol{w}_\Sigma^H\tilde{\boldsymbol{a}}\left(\theta_0, \varphi_0+\Delta\varphi'\right) \\ 0 \\ \left(-k_3\Delta\varphi'\right)\boldsymbol{w}_\Sigma^H\tilde{\boldsymbol{a}}\left(\theta_0, \varphi_0-\Delta\varphi'\right) \end{bmatrix}^T \tag{34}$$

$$\boldsymbol{\rho}_{a(\theta_0-\Delta\theta')} = \begin{bmatrix} \left(-k_2\Delta\theta'+k_3\Delta\varphi'\right)\boldsymbol{w}_\Sigma^H\tilde{\boldsymbol{a}}\left(\theta_0-\Delta\theta', \varphi_0+\Delta\varphi'\right) \\ \left(-k_2\Delta\theta'\right)\boldsymbol{w}_\Sigma^H\tilde{\boldsymbol{a}}\left(\theta_0-\Delta\theta', \varphi_0\right) \\ \left(-k_2\Delta\theta'-k_3\Delta\varphi'\right)\boldsymbol{w}_\Sigma^H\tilde{\boldsymbol{a}}\left(\theta_0-\Delta\theta', \varphi_0-\Delta\varphi'\right) \end{bmatrix}^T \tag{35}$$

$$\boldsymbol{\rho}_{e(\theta_0+\Delta\theta')} = \begin{bmatrix} \left(k_1\Delta\varphi'\right)\boldsymbol{w}_\Sigma^H\tilde{\boldsymbol{a}}\left(\theta_0+\Delta\theta', \varphi_0+\Delta\varphi'\right) \\ 0 \\ -\left(k_1\Delta\varphi'\right)\boldsymbol{w}_\Sigma^H\tilde{\boldsymbol{a}}\left(\theta_0+\Delta\theta', \varphi_0-\Delta\varphi'\right) \end{bmatrix}^T \tag{36}$$

$$\boldsymbol{\rho}_{e(\theta_0)} = \begin{bmatrix} \left(k_1\Delta\varphi'\right)\boldsymbol{w}_\Sigma^H\tilde{\boldsymbol{a}}\left(\theta_0, \varphi_0+\Delta\varphi'\right) \\ 0 \\ -\left(k_1\Delta\varphi'\right)\boldsymbol{w}_\Sigma^H\tilde{\boldsymbol{a}}\left(\theta_0, \varphi_0-\Delta\varphi'\right) \end{bmatrix}^T \tag{37}$$

$$\boldsymbol{\rho}_{e(\theta_0+\Delta\theta')} = \begin{bmatrix} \left(k_1\Delta\varphi'\right)\boldsymbol{w}_\Sigma^H\tilde{\boldsymbol{a}}\left(\theta_0-\Delta\theta', \varphi_0+\Delta\varphi'\right) \\ 0 \\ -\left(k_1\Delta\varphi'\right)\boldsymbol{w}_\Sigma^H\tilde{\boldsymbol{a}}\left(\theta_0-\Delta\theta', \varphi_0-\Delta\varphi'\right) \end{bmatrix}^T \tag{38}$$

As mentioned earlier, the adaptive azimuth and elevation difference beam weights, i.e., $\bar{\boldsymbol{w}}_{\Delta a}$ and $\bar{\boldsymbol{w}}_{\Delta e}$, are required not only to guarantee the approximation between the adaptive and conventional quiescent monopulse ratios as shown in (26), but also to minimize the power of the received jammings and noise. As a result, the determination of $\bar{\boldsymbol{w}}_{\Delta a}$ and $\bar{\boldsymbol{w}}_{\Delta e}$ can be formulated as the following optimization problems:

$$\begin{aligned} \min_{\bar{\boldsymbol{w}}_{\Delta a}} \quad & \bar{\boldsymbol{w}}_{\Delta a}^H\hat{\boldsymbol{R}}_{\text{sub}}\bar{\boldsymbol{w}}_{\Delta a} \\ \text{s.t.} \quad & \bar{\boldsymbol{w}}_{\Delta a}^H\boldsymbol{H} = \boldsymbol{\rho}_a \end{aligned} \tag{39}$$

and

$$\begin{aligned} \min_{\bar{\boldsymbol{w}}_{\Delta e}} \quad & \bar{\boldsymbol{w}}_{\Delta e}^H\hat{\boldsymbol{R}}_{\text{sub}}\bar{\boldsymbol{w}}_{\Delta e} \\ \text{s.t.} \quad & \bar{\boldsymbol{w}}_{\Delta e}^H\boldsymbol{H} = \boldsymbol{\rho}_e. \end{aligned} \tag{40}$$

Interestingly, it is observed that the above two problems can be viewed as linearly constrained minimum variance (LCMV) beamformers[1][24]. Moreover, the adaptive difference weights $\bar{\boldsymbol{w}}_{\Delta a}$ and $\bar{\boldsymbol{w}}_{\Delta e}$ can be obtained by solving (39) and (40) with the Lagrange's multiplier method as

$$\bar{\boldsymbol{w}}_{\Delta a} = \hat{\boldsymbol{R}}_{\text{sub}}^{-1}\boldsymbol{H}(\boldsymbol{H}^H\hat{\boldsymbol{R}}_{\text{sub}}^{-1}\boldsymbol{H})^{-1}\boldsymbol{\rho}_a^H \tag{41a}$$

$$\bar{\boldsymbol{w}}_{\Delta e} = \hat{\boldsymbol{R}}_{\text{sub}}^{-1}\boldsymbol{H}(\boldsymbol{H}^H\hat{\boldsymbol{R}}_{\text{sub}}^{-1}\boldsymbol{H})^{-1}\boldsymbol{\rho}_e^H. \tag{41b}$$

It can be seen from the above derivations that the proposed difference weights in (41) fulfill the conditions given in (25), and therefore, they are able to maintain the linearity of the monopulse ratios. Since constraints on both of the azimuth and elevation are considered in the proposed approach, relatively better angle measuring performance can be achieved. This will be verified by simulations results in the following section.

V. NUMERICAL RESULTS

To demonstrate the performance of the proposed approach, several sets of simulation results are provided. We first consider the surface of adaptive monopulse ratio in the case of a mainlobe jammer. Next, the angle measuring performance of the proposed method is illustrated and compared with that of the conventional MVDR monopulse method, the corrected monopulse method in [9] and constrained monopulse algorithm in [19]. Finally, we illustrate the influence of the constraint interval and the constraint number on angle measuring performance.

In all simulations, we assume a planar array with 16×16 elements, the array element spacing is $d_y = d_z = 0.5\lambda$, and the array is partitioned into 4×4 subarrays. The signal-to-noise ratio is 20 dB and the interference-to-noise ratio is assumed to be 40 dB for all jammers. The number of training samples is $K = 100$, and $L = 1000$ Monte Carlo simulation runs have been used to obtain each point.

[1] It is remarkable that the adaptive implementations of the LCMV estimator have been developed resorting to constrained stochastic gradient [25], constrained recursive least squares [26], [27], and constrained Kalman-type [28] algorithms. The equivalence between the LCMV estimator and the generalized side lobe canceller processor [29]–[31] allows to resort as well to standard (unconstrained) stochastic gradient or recursive least squares [32].

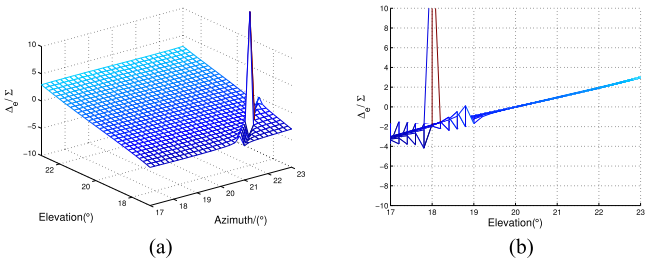

Fig. 4. Surface of adaptive elevation monopulse ratio. (a) Oblique view. (b) Side view.

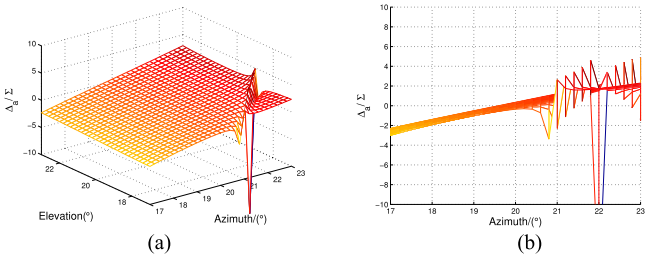

Fig. 5. Surface of adaptive azimuth monopulse ratio. (a) Oblique view. (b) Side view.

A. Surfaces of the Adaptive Monopulse Ratios

Assume that the constraint interval is $(\Delta\theta', \Delta\varphi') = (3^\circ, 3^\circ)$ and 3×3 uniform interval constraints are considered. Furthermore, assume that the look direction is $(20^\circ, 20^\circ)$, one sidelobe jammer locates at $(-30^\circ, -30^\circ)$, and one mainlobe jammer locates at $(22^\circ, 18^\circ)$ with respect to broadside. Figs. 4 and 5 show the resulting surfaces of the proposed adaptive monopulse.

Comparing Fig. 4(b) with Fig. 2(b), it can be noted that the projection of the proposed elevation monopulse ratio surface on the elevation is a linear function of the elevation, except for few points that are in the vicinity of the mainlobe jammer. Moreover, comparing Fig. 5(b) with Fig. 3(b), it is seen that the projection of the proposed azimuth monopulse ratio surface on the azimuth is an approximated linear function of the azimuth and elevation except for few points. These results indicate that the surfaces of the proposed adaptive monopulse are close to those of the conventional quiescent monopulse.

B. Performance of Angle Measuring

Now, the look direction is assumed to be $(10^\circ, 10^\circ)$ and two jammers locate at $(-30^\circ, -30^\circ)$ and $(11.5^\circ, 11.5^\circ)$, respectively. The performance of the proposed method is measured in terms of the root mean square error (RMSE) of angle estimation, which is defined as

$$\mathrm{RMSE}_\theta = \sqrt{\frac{1}{L}\sum_{l=1}^{L}(\hat{\theta}_l - \theta)^2} \tag{42a}$$

$$\mathrm{RMSE}_\varphi = \sqrt{\frac{1}{L}\sum_{l=1}^{L}(\hat{\varphi}_l - \varphi)^2} \tag{42b}$$

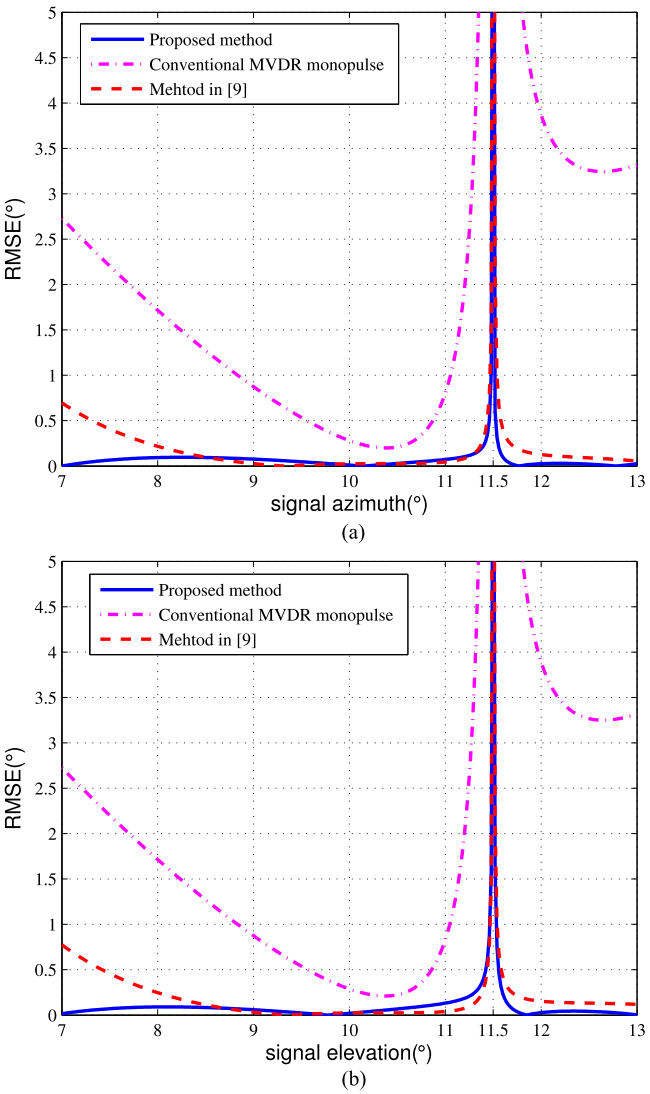

Fig. 6. RMSEs of angle measuring versus the target DOAs. 3×3 uniform interval constraints, and the constraint interval is $(\Delta\theta', \Delta\varphi') = (3^\circ, 3^\circ)$. (a) Azimuth. (b) Elevation.

where L is the number of Monte Carlo simulations, $\hat{\theta}_l$ ($\hat{\varphi}_l$) is the estimated azimuth (elevation) in the lth simulation run, and θ (φ) is the true value of the target azimuth (elevation).

The following methods are tested for comparison: the conventional MVDR monopulse method, the corrected monopulse method in [9], and the proposed method with joint linear constraints. As can be seen from Fig. 6, the proposed approach significantly outperforms the conventional MVDR monopulse method and achieves a high angle measuring precision except for the points where the target is in the vicinity of the mainlobe jammer. Moreover, it is seen that the proposed method performs better than the corrected monopulse method when the target is in the mainlobe but significantly deviates from the look direction.

To further illustrate the superiority of the proposed approach in angle measuring, the constrained monopulse algorithm in [19] is tested. The look direction is assumed to be $(\theta_0, \varphi_0) = (10^\circ, 10^\circ)$ and the constraint interval of

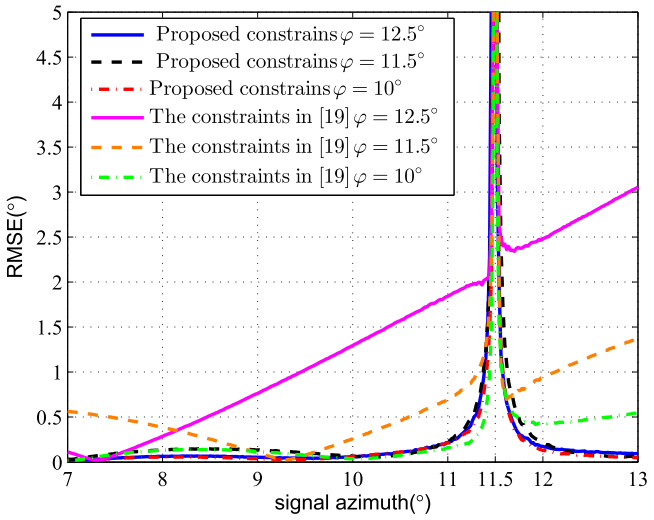

Fig. 7. RMSEs of angle measuring versus target azimuth.

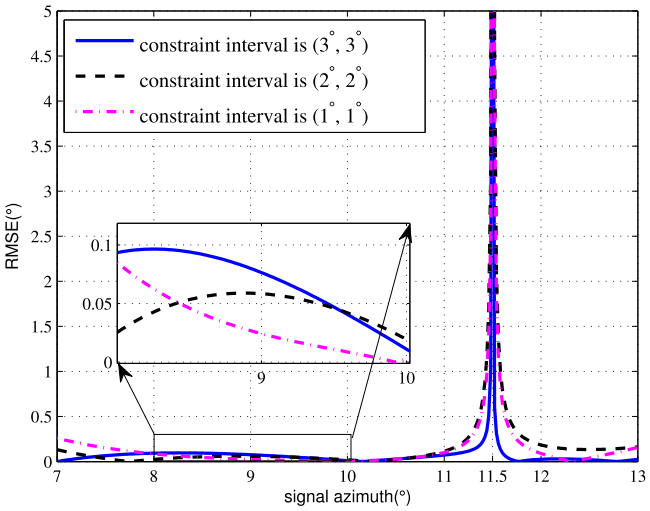

Fig. 8. RMSEs of angle measuring versus the target DOAs. 3 × 3 uniform interval constraints.

the approach is chosen to be $(\Delta\theta, \Delta\varphi) = (3°, 0.1°)$ as suggested in [19]. Three cases with different mainlobe jammer angles, i.e., (11.5°, 10°), (11.5°, 11.5°), and (11.5°, 12.5°), are considered. The RMSEs of azimuth estimates versus the target azimuth are plotted in Fig. 7 for three fixed elevation angles 10°, 11.5°, and 12.5°.

It is seen from Fig. 7 that the recent approach [19] performs well in azimuth estimation when the target elevation is equal to the look elevation, i.e., $\varphi = \varphi_0$. However, the azimuth estimation performance will be degraded if the target elevation deviates from the look elevation. The main reason is that this method ignores the dependence of the adaptive azimuth difference beam weight on both azimuth and elevation. As expected, the proposed method achieves relatively better performance than that of the approach [19].

C. Selection of the Constraint Interval

In this subsection, the influence of the constraint interval $(\Delta\theta', \Delta\varphi')$ on the angle measuring performance is evaluated. The look direction is (10°, 10°), two jammers locate at (−30°, −30°) and $(11.5°, 11.5°)$, respectively. Three constraint intervals, i.e., (3°, 3°), (2°, 2°), and (1°, 1°), are considered. The results are shown in Fig. 8.

It is observed that when the constraint interval is (3°, 3°), the proposed method obtains the highest angle measuring precision at the points that are far away from the look direction. However, when the constraint interval is (1°, 1°), the proposed method performs best for the whole constraint interval of interest. This implies that a reasonable constraint interval should be determined according to the priori information of the target direction.

D. Selection of the Number of Constraints

In this subsection, the influence of the number of constraints on the angle measuring performance is examined. It is assumed the look direction is (10°, 10°) and the incidence angles of five jammers are (−40°, −40°), (−30°, −30°), $(11.5°, 11.5°)$, (30°, 30°), and (40°, 40°). The constraint interval is $(\Delta\theta', \Delta\varphi') = (3°, 3°)$.

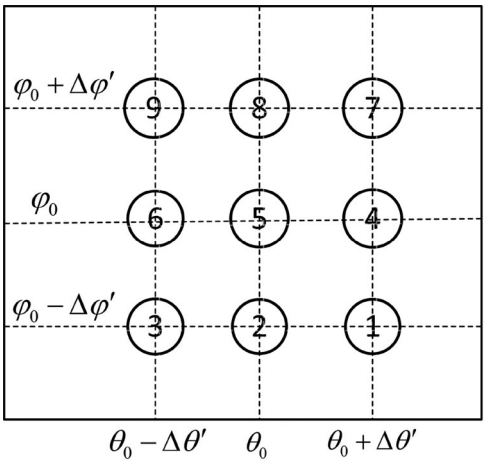

Fig. 9. Distribution of the 9-point constraint.

We compare the angle measuring performances corresponding to three selections of the number of constraints: 9-point constraint, 7-point constraint, and 5-point constraint. The distribution of the 9-point constraint is shown in Fig. 9. The 7-point constraint includes ①-③-④-⑤-⑥-⑦-⑨, whereas 5-point constraint is ①-③-⑤-⑦-⑨.

Fig. 10 displays the angle measuring performance of three different numbers of constraints (azimuth plots only). We can see that, among the three selections, the 7-point constraint achieves the best performance. This is because the angle measuring precision depends on the linearity of the surface as well as the interference suppressing. The more constraints are selected to keep the monopulse slopes unchanged on the whole intervals, the less remaining degrees of freedom are available to suppress interference.

Fig. 11 shows that the interference suppressing performance in terms of the output SINR. It can be seen that the SINR of the 5-point constraint is more prominent than the other two cases. Moreover, the performance will be

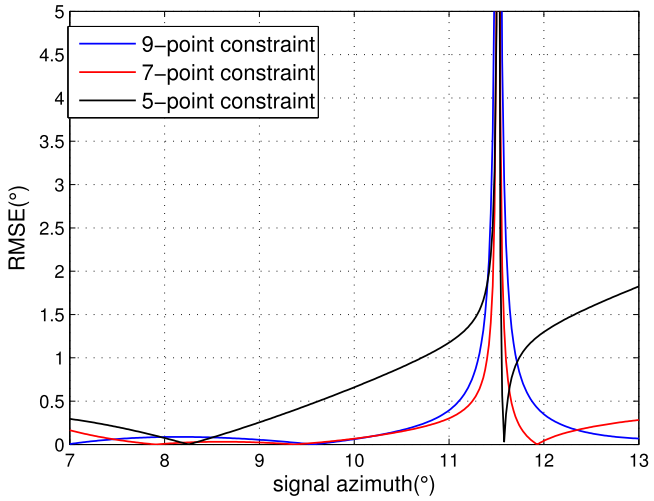

Fig. 10. RMSEs of angle measuring versus the target DOAs. The constraint interval is $(\Delta\theta', \Delta\varphi') = (3^\circ, 3^\circ)$.

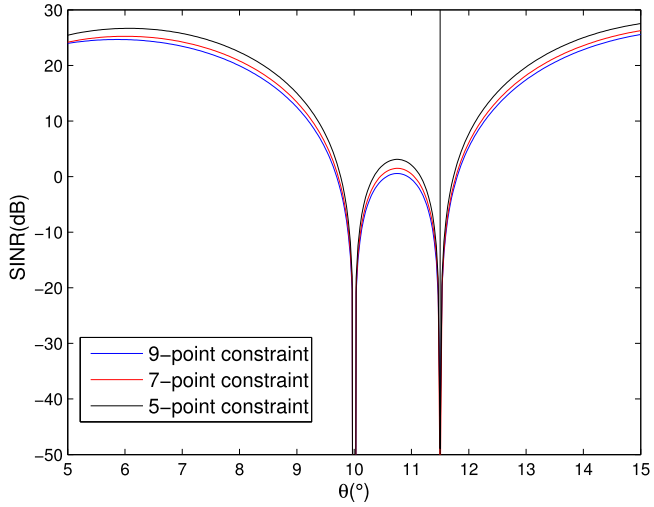

Fig. 11. Output SINR of the azimuth difference adaptive weight.

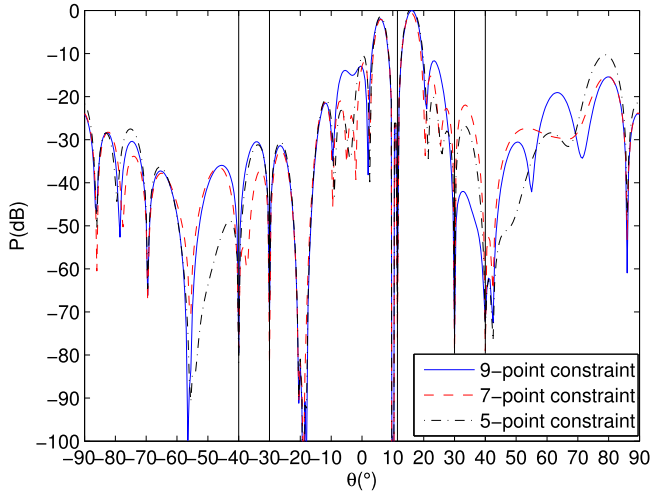

Fig. 12. Pattern of the azimuth difference adaptive weight.

seriously degraded at those two points where the angle of the target is equal to the look direction and the angle of the mainlobe jammer, since the difference pattern should be zero at the look direction as shown in Fig. 12. Therefore, in practical applications, the number of constraints should be properly selected according to specific jamming scenarios.

VI. CONCLUSION

In this paper, the problem of angle measuring with a planar array partitioned into subarrays is considered. To improve the performance in jamming environment, we have proposed a new adaptive monopulse approach with joint linear constraints on the azimuth and elevation such that the adaptive monopulse ratio surfaces are approximated to the conventional quiescent monopulse ratio surfaces. It has been shown that the monopulse ratios can be constrained flexibly according to different look directions. The performance of the proposed method is measured in terms of the RMSE of angle estimation. It is found that the proposed method is able to obtain a high angle measuring precision in the presence of mainlobe jammer. Moreover, discussions about the constraint interval, the number of constraints and comparison with adaptive monopulse are carried out to investigate the proposed approach.

ACKNOWLEDGMENT

The authors thank Associate Editor Dr. A. Charlish for carefully coordinating the review of this paper and the anonymous referees for interesting and pertinent comments.

REFERENCES

[1] I. Reed, J. Mallett, and L. Brennan
Rapid convergence rate inadaptive arrays
IEEE Trans. Aerosp. Electron. Syst., vol. AESC10, pp. 853–863, Nov. 1974.

[2] L. Brennan and I. Reed
Theory of adaptive radar
IEEE Trans. Aerosp. Electron. Syst., vol. AES-9, no. 2, pp. 237–252, Mar. 1973.

[3] M. Zoltowski
Synthesis of sum and difference patterns processing common nulls for monopulse bearing estimation with line array
IEEE Trans. Antennas Propag., vol. 40, no. 1, pp. 25–37, Jan. 1992.

[4] R. Davis, L. Brennan, and I. Reed
Angle estimation with adaptive arrays in external noise fields
IEEE Trans. Aerosp. Electron. Syst., vol. AES-12, no. 2, pp. 179–186, Mar. 1976.

[5] U. Nickel
Overview of generalized monopulse estimation
IEEE Aerosp. Electron. Syst. Mag., vol. 21, no. 6, pp. 27–56, Jun. 2006.

[6] J. Wu, T. Wang, and Z. Bao
Angle estimation for adaptive linear array using PCA-GS-ML estimator
IEEE Trans. Aerosp. Electron. Syst., vol. 49, no. 1, pp. 670–677, Jan. 2013.

[7] U. Nickel
Monopulse estimation with adaptive arrays
IEE Proc. - Radar Sonar Navig., vol. 140, no. 5, pp. 303–308, Oct. 1993.

[8] U. Nickel
Array processing for radar: Achievements and challenges
Int. J. Antennas Propag., vol. 2013, pp. 1396–1399, 2013.

[9] U. Nickel
Monopulse estimation with subarray-adaptive arrays and arbitrary sum and difference beams
IEE Proc.-Radar Sonar Navig., vol. 143, no. 4, pp. 232–238, Aug. 1996.

[10] U. Nickel
Subarray configurations for digital beamforming with low sidelobes and adaptive interference suppression
In *Proc. IEEE Int. Radar Conf.*, Alexandria, VA, USA, May 1995, pp. 714–719.

[11] U. Nickel
Monopulse estimation with subarray output adaptive beamforming and low sidelobe sum and difference beams
In *Proc. Int. Symp. Phased Array Syst. Technol.*, Boston, MA, USA, 1996, pp. 283–288.

[12] R. Klemm and U. Nickel
Adaptive monopulse with STAP
In *Proc. IEEE Radar Conf.*, New York, NY, USA, Apr. 24–27, 2006, pp. 1–4.

[13] Y. Seliktar, E. Holder, and D. Williams
An adaptive monopulse processor for angle estimation in a mainbeam jamming and coherent interference scenario
In *Proc. IEEE Int. Conf. Acoust. Speech Signal Process.*, Seattle, WA, USA, 1998, pp. 2037–2040.

[14] U. Nickel, E. Chaumette, and P. Larzabal
Statistical performance prediction of generalized monopulse estimation
IEEE Trans. Aerosp. Electron. Syst., vol. 47, no. 1, pp. 381–404, Jan. 2011.

[15] R. Wu, Z. Su, and L. Wang
Space-time adaptive monopulse processing for airborne radar in non-homogeneous environments
AEU-Int. J. Electron. Commun., vol. 65, pp. 258–264, 2011.

[16] A. Paine
Application of the minimum variance monopulse technique to space-time adaptive processing
In *Proc. IEEE Int. Conf. RADAR 2000*, Alexandria, VA, USA, May 2000, pp. 596–601.

[17] K. Yu and D. Murrow
Adaptive digital beamforming for angle estimation in jamming
IEEE Trans. Aerosp. Electron. Syst., vol. 37, no. 2, pp. 508–523, Apr. 2001.

[18] R. Fante
Synthesis of adaptive monopulse
IEEE Trans. Antennas Propag., vol. 47, no. 5, pp. 773–774, May 1999

[19] X. Zhang
et al. A novel monopulse technique for adaptive phased array radar
Sensors, vol. 17, no. 1, 2017, doi: 10.3390/s17010116.

[20] R. Monzingo and T. Miller
Introduction to Adaptive Arrays. New York, NY, USA: Wiley, 1980.

[21] M. Zoltowski
On the performance of the MVDR beamformer in the presence of correlated interference
IEEE Trans. Acoust. Speech Signal Process., vol. 36, no. 6, pp. 945–947, Jun. 1988.

[22] I. Reed, J. Mallett, and L. Brennan
Rapid convergence rate in adaptive arrays
IEEE Trans. Aerosp. Electron. Syst., vol. 10, no. 6, pp. 853–863, Nov. 1974.

[23] S. A. Vorobyov
Principles of minimum variance robust adaptive beamforming design
Signal Process., vol. 93 pp. 3264–3277, 2013.

[24] H. Trees
Optimum Array Processing. New York, NY, USA: Wiley-Interscience, 2002.

[25] O. L. Frost
An algorithm for linearly constrained adaptive array processing
Proc. IEEE, vol. 60, no. 8 pp. 926–935, Aug. 1972.

[26] L. Resende, J. Romano, and M. Bellanger
Fast least squares algorithm for linearly constrained adaptive filtering
IEEE Trans. Signal Process., vol. 44, no. 5, pp. 1168–1174, May 1996.

[27] R. Lamare
Adaptive reduced-rank LCMV beamforming algorithms based on joint iterative optimisation of filters
Electron. Lett., vol. 44, no. 8, pp. 565–566, 2008.

[28] Y. Chen and C. Chiang
Adaptive beamforming using the constrained Kalman filter
IEEE Trans. Antennas Propag., vol. 41, no. 11, pp. 1576–1580, Nov. 1993

[29] L. Griffiths and C. Jim
An alternative approach to linearly constrained adaptive beamfonning
IEEE Trans. Antennas Propag., vol. 30, no. 1, pp. 27–34, Jan. 1982.

[30] B. Breed and J. Strauss
A short proof of the equivalence of LCMV and GSC beamforming
IEEE Signal Process. Lett., vol. 9, no. 6, pp. 168–169, Jun. 2002.

[31] S. Werner, J. Apolinario Jr, and M. De Campos
On the equivalence of RLS implementations of LCMV and GSC processors
IEEE Signal Process. Lett., vol. 10, no. 12, pp. 356–359, Dec. 2003.

[32] Paulo S. R. Diniz
Adaptive Filtering: Algorithms and Practical Implementation, 4th ed. New York, NY, USA: Springer-Verlag, 2013.

Ziyang Cheng (S'17) was born in Yingcheng, Hubei, China, in 1990. He received the M.S. degree in circuits and systems from the University of Electronic Science and Technology of China (UESTC), Chengdu, China, in 2015. He is currently working toward the Ph.D. degree in signal and information processing at the UESTC.

His research interests include array signal processing, MIMO radar waveform design, radar target detection, and optimization theory.

Zishu He (M'11) was born in Chengdu, Sichuan province, China in 1962. He received the B.S., M.S., and Ph.D. degrees in signal and information processing from the University of Electronic Science and Technology of China (UESTC), Chengdu, China, in 1984, 1988, and 2000, respectively.

He is currently a Professor with the School of Electronic Engineering, UESTC. He has authored or coauthored more than two hundred papers and has written two books. His current research interests include array signal processing, digital beam forming, the theory on MIMO radar, and adaptive signal processing.

Xiang Duan received the B.S. and Ph.D. degrees in signal and information processing from the School of Electronic Engineering, University of Electronic Science and Technology of China (UESTC), Chengdu, China, in 2009 and 2017, respectively.

His research interests include array signal processing and MIMO radar system design.

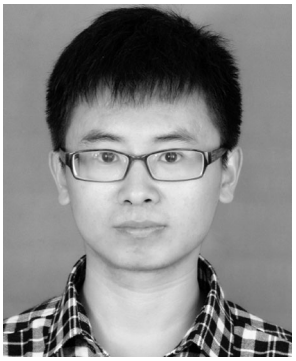

Xuejing Zhang (S'17) was born in Hebei, China. He received the B.S. degree in electrical engineering from Huaqiao University, Xiamen, China, and the M.S. degree in signal and information processing from Xidian University, Xi'an, China, in 2011 and 2014, respectively. He is currently working toward the Ph.D. degree in signal and information processing at the Department of Electronic Engineering, University of Electronic Science and Technology of China, Chengdu, China.

Since November 2017, he has been a visiting student with the University of Delaware, Newark, DE, USA. From 2014 to 2015, he was a Research Engineer with the Allwinner Inc., Zhuhai, China, where he was engaged in algorithmic research. His research interests include array signal processing, optimization theory, and machine learning.

Bin Liao (S'09–M'13–SM'16) received the B.Eng. and M.Eng. degrees in electronic engineering from Xidian University, Xian, China, in 2006 and 2009, respectively, and the Ph.D. degree in electronic engineering from The University of Hong Kong, Hong Kong, in 2013.

From September 2013 to January 2014, he was a Research Assistant with the Department of Electrical and Electronic Engineering, The University of Hong Kong, Hong Kong. From August 2016 to October 2016, he was a Research Scientist with the Department of Electrical and Electronic Engineering, The University of Hong Kong, Hong Kong. He is currently an Associate Professor with the College of Information Engineering, Shenzhen University, Shenzhen, China. His research interests include sensor array processing, adaptive filtering, convex optimization, with applications to radar, navigation and communications.

Dr. Liao is an Associate Editor for *IET Signal Processing, Multidimensional Systems and Signal Processing*, and IEEE ACCESS. He was the recipient of the Best Paper Award at the 21st International Conference on Digital Signal Processing (2016 DSP) and 22nd International Conference on Digital Signal Processing (2017 DSP).